Electrospun carbon nanofibers with in-situ encapsulated Ni nanoparticles as catalyst for enhanced hydrogen storage of MgH_2

Qiufang Meng [a], Yuqin Huang [b], Jikai Ye [b], Guanglin Xia [b], Gaofeng Wang [a], Linxi Dong [a, **], Zunxian Yang [c, ***], Xuebin Yu [b, a, *]

[a] Key Laboratory of RF Circuits and System of Ministry of Education, Electronic and Information College of Hangzhou Dianzi University, Hangzhou, 310018, China
[b] Department of Materials Science, Fudan University, Shanghai, 200433, China
[c] National & Local United Engineering Laboratory of Flat Panel Display Technology, Fuzhou University, Fuzhou, 350002, China

ARTICLE INFO

ABSTRACT

Transition-metals have emerged as promising catalyst candidates for improving the hydrogen storage properties of MgH2. However, the preparation of uniformly dispersed and extra-fine transition-metals catalysts with high catalytic activity still remains a challenge. In this paper, an electrospinning-based reduction approach is presented to generate nanostructured nickel catalyst, which is protected from irreversible fusion and aggregation in subsequent high-temperature pyrolysis, in carbon nanofibers (Ni@C) in situ. The obtained Ni@C reveals remarkable catalytic effect on improving the hydrogen storage properties of MgH2. For example, the MgH2-10 wt%Ni@C composite delivers dehydrogenation capacities of 5.79 wt% and 6.12 wt% at 280 °C and 300 °C, respectively, whereas the as-milled MgH2 hardly decomposes at the same temperature. By Arrhenius plots, the calculated Ea of the dehydrogenation of MgH2-10 wt%Ni@C is 93.08 kJ mol−1, which is 94.33 kJ mol−1 lower than that of the as-milled MgH2. Furthermore, the microstructure of Ni@C is remained during the re/dehydrogenation process and the Ni nanoparticles are still distributed homogeneously in the composite, accounting for the excellent cycling performance. This study could render combinations of ultrafine metal nanoparticles with carbon accessible, thereby, extending opportunities in catalytic applications for hydrogen storage.

© 2020 Elsevier B.V. All rights reserved.

1. Introduction

Hydrogen (H2) with its renewable, green, clean properties and high-energy density, has gained a great attention as an ideal sustainable candidate for the alternative energy sources to replace fossil fuels [1−9]. However, the widespread use of hydrogen in practical applications is severely limited by the relatively backward hydrogen storage technologies [10,11]. Currently, except for the successful application of hydrogen storage alloys in Ni-MH batteries [12−16], few developed hydrogen storage materials can meet the requirement of practical application, particularly for the on-

board applications targets proposed by the U. S. Department of Energy (DOE) [17]. As a typical solid-state hydrogen storage material, magnesium hydride (MgH2) with high theoretical hydrogen capacities (7.6 wt% in gravimetry and 110 kg/m3 in volumetric), excellent reversibility, abundance, and low cost has attracted great attentions in the past decades [18−21]. Nevertheless, the drawbacks of high hydrogenation/dehydrogenation temperature and low hydrogen desorption/absorption rate resulted from the thermodynamic stability and slow kinetics, need to be overcome before its practical application in on-board fuel cells. Thus, tuning these two intrinsic parameters in absorption/desorption reaction are the keys in improving the hydrogen storage performances of materials [22−24].

To improve the hydrogen storage properties of MgH2, different strategies including alloying [25−30], catalyzing [31−35] and nanosizing [36−41] have been developed and demonstrated impressive improvements, among which catalyzing is one of the most effective methods. A variety of different catalysts, such as

carbon materials, metals and intermetallics, transition-metal compounds (oxides, halides, hydrides, carbides, nitrides and fluorides) have been reported to enhance the hydrogen storage properties of Mg-based materials [42–49]. Particularly, transition metal-related catalytic systems, e.g. Ni-based catalysts, have shown superior properties in improving the adsorption kinetics and promoting the rapid and effective dissociation or recombination of hydrogen molecules in Mg-based materials. For example, Yao et al. [50] developed a one-step method to capitalize on the in situ bottom-up reduction of a Ni-MOF-74 precursor in the presence of MgH2 as a reducing and sacrificial agent via mechanical chemical ball milling, and the MgH2-5 wt% (Ni-MOF-74) composite can absorb 6.2 wt% hydrogen within only 30 s at a temperature as low as 150 °C. Jalil et al. [51] proposed a new technique to study MgH2 catalyzed with a small amount of Ni nanoparticles by the reactive ball milling under 10 bar hydrogen. The results showed that the MgH2-2 mol% Ni nanopowders could absorption/desorption 5.3 wt % H2 within 5 min, exhibiting that a small amount of Ni with nanoscale could be a suitable catalyst for improving the kinetics of MgH2. Wang et al. [52] developed a self-template strategy using benzimidazole as the reductant and carbon precursor to fabricated Ni@C and the desorption peak temperature of the MgH2–Ni@C composite was lowered down to 283 °C. Li et al. [44] prepared Mg and Ni nanoparticles by hydrogen plasma-metal reaction (HPMR) and the MgH2 nanoparticles were obtained by hydriding the Mg nanoparticles. The obtained sample showed superior hydrogen storage kinetics, releasing 6.1 wt% hydrogen in 10 min at 250 °C under an initial pressure of 0.01 bar of H2 when the proportion of Ni nanoparticles is 10 wt%. It is drawn that the enhanced desorption kinetics are mainly attributed to the accelerated combination process of hydrogen atoms by the Ni nanoparticles on the surface of MgH2.

Compared with bare nano-Ni, carbon supported nano-Ni catalysts could exhibit better catalytic effect on improving the hydrogen storage properties of MgH2, since Ni nanoparticles can be distributed uniformly on the surface of carbon matrix and the microstructure is able to remain well during the following process to ensure the stability of the catalysts. Therefore, preparing uniformly dispersed and extra-fine Ni-based catalyst with high catalytic activity is of significant value to the application of MgH2. Many efforts have been devoted toward realizing metallic compounds as catalysts, including with the use of carbon nanotubes [34], active carbon, graphene [53–55], and carbon nanofibers (CNFs) [46] as substrates. Among these substrates, CNFs embraced with some intrinsic advantages, such as large surface area, lightweight, good electrical conductivity, and high thermal/chemical/mechanical stability, have been allured a great deal of attention in eminent researchers [56,57].

Herein, we describe an in situ preparation of embedded ultrafine Ni nanoparticles in carbon nanofibers (Ni@C) by electrospinning technique, followed by controllable pyrolyzed reduction in a H2/Ar atmosphere. In our method, a precise ratio of nickel cation and polyvinylpyrrolidone (PVP) was well mixed and then electrospun into 1D NFs. In the subsequent pyrolysis reduction, Ni cation was transformed into Ni nanoparticles and then embedded in the carbon matrix. The accompanying ultrafine porosity resulted from the decomposition of PVP were used as a molecular sieve to effectively prevent the aggregation of the in situ generated Ni nanoparticles, which is beneficial to confine Ni nanoparticles to a very small size (ca. 5 nm in diameter). As a result, the Ni-catalyzed MgH2 exhibits significantly improved hydrogen storage properties.

2. Experimental

2.1. Syntheses of Ni@C and MgH2−Ni@C composite

Chemicals were all obtained commercially and used without any purification. MgH2 (98% in purity) was purchased from Alfa Aesar. Nickel nitrate hexahydrate (Ni(NO3)2·6H2O) and polyvinylpyrrolidone (PVP, Mw ~ 1300000) were purchased from A.R., Alfa-Aesar Inc., USA and Sigma-Aldrich Inc, USA) respectively. *N,N*-dimethylformamide (DMF) and ethanol were both purchased from A.R., Tianjin Chemical Corp., China.

2.1.1. Syntheses of Ni@C

Carbon supported Ni catalyst was synthesized via the following procedure.

Polyvinylpyrrolidone (PVP, 0.17 g) and nickel nitrate hexahydrate (Ni(NO3)2·6H2O, 0.101 g) was dispersed in 1.25 ml of ethanol and 1.25 ml of DMF, with vigorous stirring for 24 h to make a homogeneous spinning dope. After that, the well-prepared precursor solution was poured into a syringe with an 18-gauge blunt-tipped needle. The voltage, which was provided by a high-voltage power supply, and the distance between the needle and the collector were set at 12 kV and 15 cm, respectively. The flow rate of the solution was controlled by a syringe pump (Longer, TJP-3A, China) to approximately 250 μl h-1. Then the as-collected fibers produced by electrospinning were annealed in air at 250 °C with a heating rate of 2 °C min-1 for 3 h, and finally carbonized in hydrogen/argon atmosphere at 400 °C with a heating rate of 3 °C min-1 for 3 h to obtain the porous Ni@C nanofibers.

2.1.2. MgH2−Ni@C composite

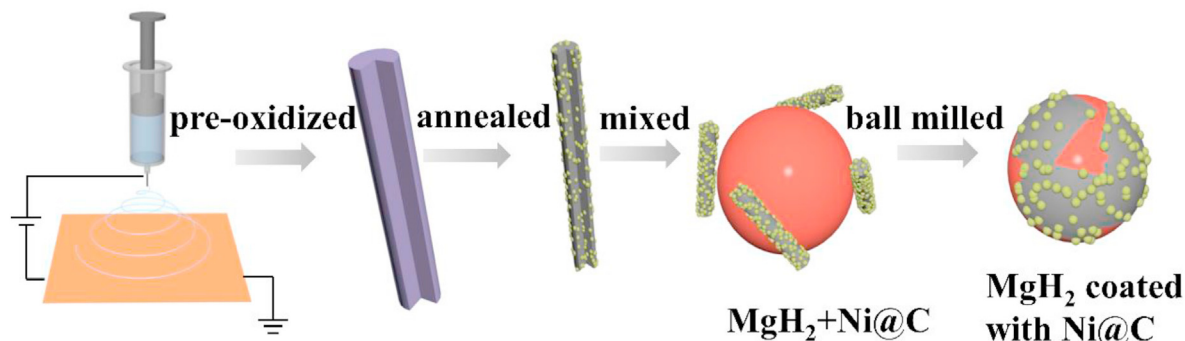To prepare the MgH2−Ni@C composite, X wt% (X = 5, 10, 15 and

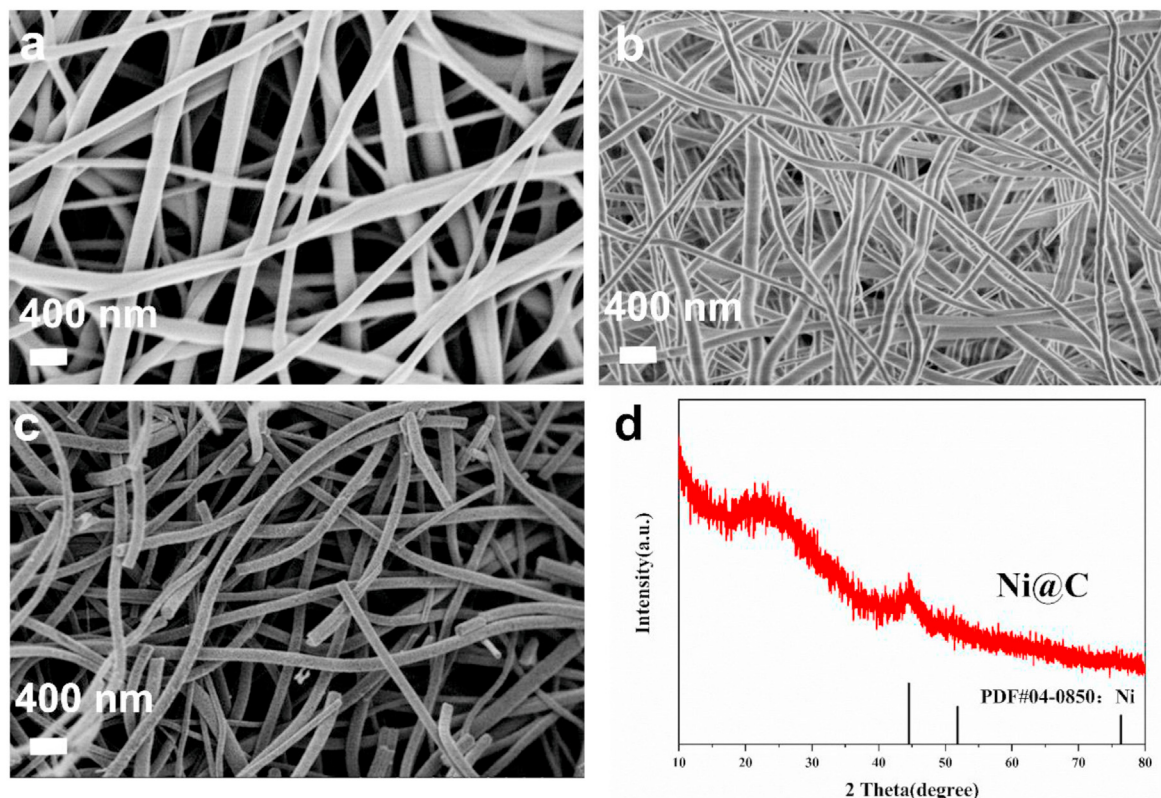**Fig. 1.** Schematic illustration for the Ni@C formation process and the synergetic catalytic effect on MgH2.

Fig. 2. SEM image of the as-electrospun PVP-coated Ni(NO3)2 nanofibers (a), pre-oxidized as-electrospun PVP-coated Ni(NO3)2 nanofibers(b), SEM image of Ni@C nanofibers (c) and XRD pattern of Ni@C synthesized by calcination (d).

20) Ni@C catalyst was added into the commercially available MgH2 (Alfa Aesar 98%) powder by mechanically milling for 10 h under Ar atmosphere using a planetary ball mill (QM- 1SP2, Nanjing). The ball-to-powder weight ratio was 50:1, and the milling speed was 350 rpm. The operation on the samples was handled in a glovebox filled with high purity argon (99.999%), which could keep the water vapor and oxygen levels below 1 ppm by recycling the purification system to protect samples from hydroxide formation and/or oxidation. The obtained samples were labeled as MgH2-X wt%Ni@C (X = 5, 10, 15 and 20). In addition, pure MgH2 without catalyst was also ball milled in the same way as a reference sample.

2.2. Sample characterizations

The phase composition of the composites was examined by X-ray diffraction (XRD, D8 Advance, Bruker AXS) with Cu Ka radiation. The structure and morphology of the samples were characterized by field emission scanning electron microscopy (FE-SEM; JEOL7500FA, Tokyo, Japan) and a transmission electron microscope (TEM; JEOL 2011 F, Tokyo, Japan). The hydrogen storage properties of the samples were measured on a HPSA-auto high pressure volume gas storage device (self-made). During the hydrogen storage performance test, about 0.1 g of each sample was loaded into a stainless steel sample chamber in the glovebox filled with argon. The initial hydrogen pressure of absorption kinetics measurements was 3.0 MPa.

Temperature-programmed desorption (TPD) was used to investigate the hydrogen desorption properties of MgH2-X wt% Ni@C at a constant heating rate of 5 °C min-1 to evaluate the catalytic effectiveness of Ni@C, and the result is presented in the following part.

3. Results and discussion

For visual presentation, Fig. 1 illustrates two processes, including the preparation of the Ni@C nanofibers and the mixing of MgH2 and Ni@C. The Ni@C nanofibers were produced by simple electrostatic spinning and controlled pyrolysis reduction in a H2 atmosphere. Briefly, polyvinylpyrrolidone (PVP) and nickel nitrate hexahydrate (Ni(NO3)2·6H2O) were mixed to an exact ratio to produce a pale green spinning precursor. The prepared precursor solution is then poured into a syringe with a No. 18 blunt needle, and the as-spun fiber matrix was obtained by an electrospinning technique. The as-spun fiber was firstly pre-oxidized in air at 250 °C for 3 h and further annealed in a H2/Ar atmosphere for 3 h. During the process, PVP was decomposed with simultaneously producing ultrafine voids, the Ni ions were transformed into metal Ni nanoparticles and embedded in the porous carbon matrix. The ultrafine voids after PVP thermal decomposition were used as molecular sieves, which prevented Ni nanocrystals from gathering in the pyrolysis and reduction process and helped to maintain the fine size of Ni particles (the average diameter was 5 nm). Because of this excellent property, the Ni nanoparticles embedded in the porous carbon fiber (Ni@C) showed prominent catalytic effects on hydrogen desorption and hydrogen adsorption of MgH2. A certain proportion of Ni@C and commercial MgH2 were mechanically mixed by high-energy ball milling. The Ni@C were uniformly dispersed on the surface of MgH2, which enhanced the interface interaction and promoted the interaction between Ni@C and MgH2.

3.1. Structural characterizations of Ni@C and the MgH2−Ni@C composite

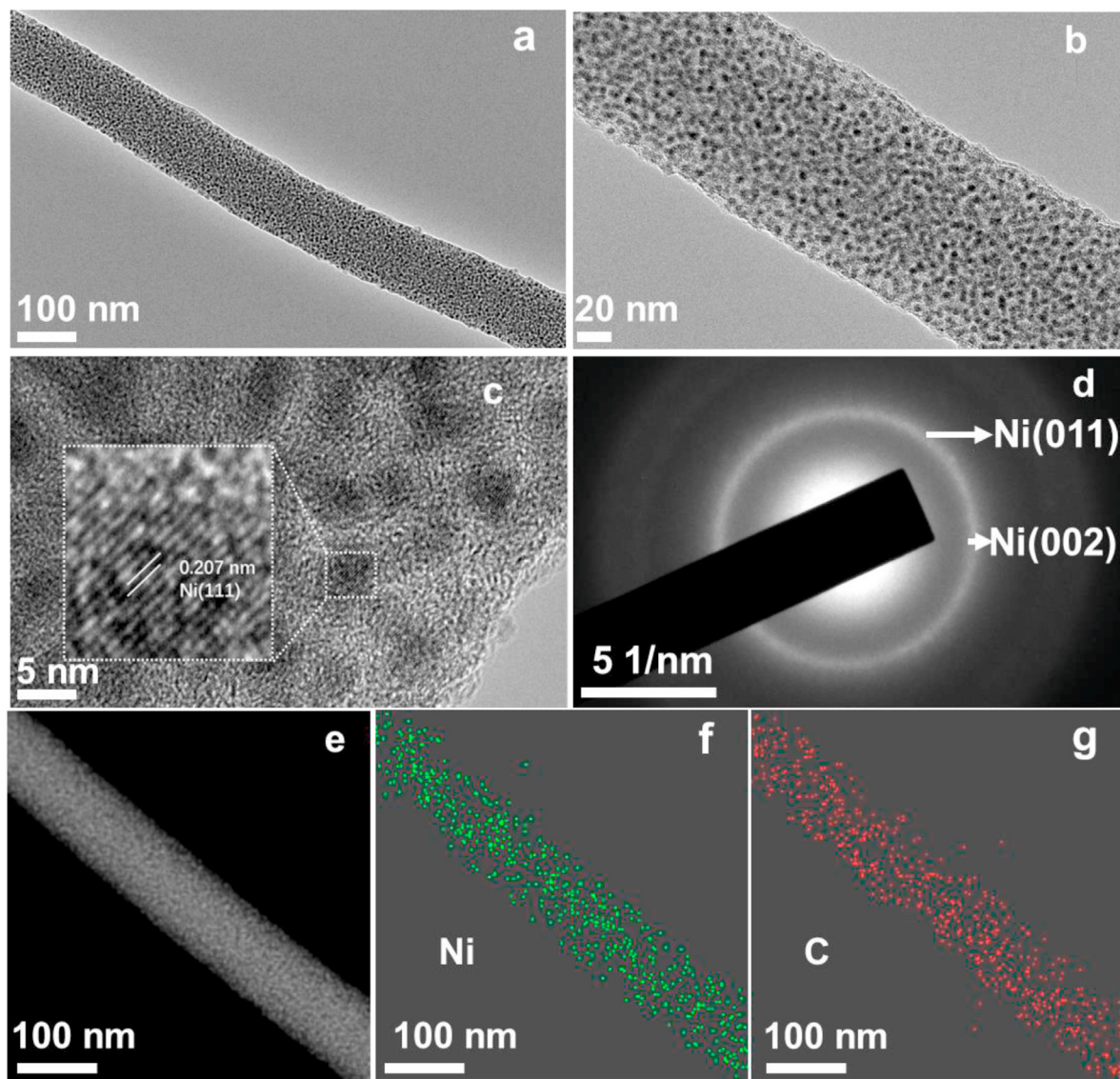The micromorphology of the corresponding products at each

Fig. 3. (a–b) TEM images, (c) HRTEM image, (d) SAED pattern and (e–g) element mapping of the as-prepared Ni@C: (f) Ni, and (g) C.

reaction stage in the synthesis of Ni@C was characterized by scanning electron microscope (SEM) as shown in Fig. 2a–c. Fig. 2a shows that the precursor fibers obtained by electrostatic spinning reveal smooth and uniform solid 1D nanofibers (NFs) structures with an average diameter of 185 nm. After pre-oxidation, the diameter of the fiber decreases to 119 nm averagely and the one-dimensional nanofiber structure is still maintained (Fig. 2b). Fig. 2c shows the SEM image of the final product (Ni@C) obtained after pyrolysis and reduction. As expected, the solid 1D structures of the nanofiber precursors are well-maintained, while the surfaces of the NFs became much rougher. The as-prepared Ni@C nanofibers are homogeneous and continuous with a shrinkable diameter of 117 nm and the fine Ni nanocrystals were uniformly dispersed in the matrix of the carbon nanofibers. After the pyrolysis reduction treatment, PVP is decomposed into fine porous carbon fibers, and the ultrafine voids as molecular sieves limit the growth and aggregation of nickel nanocrystals, resulting in a very small size of Ni nanoparticles. The X-ray diffraction (XRD) pattern of Ni@C reveals that apart from the broad diffraction hump at about 25° assigned to the amorphous carbon, the remaining diffraction peaks at 44.38°

(111), 51.84° (200), and 76.37° (220) are consistent with Ni (JCPDS no. 04–0850), and the diffraction peak shape is not obvious because of the small grain size and the poor crystallinity of Ni (Fig. 2d). No diffraction peaks corresponding to other phases or impurities are observed, indicating that this pyrolysis reduction strategy manufactures Ni successfully.

The transmission electron microscopy (TEM) images show that the Ni@C presents a pea-like structure, and the uniform Ni nanoparticles (black dots) with a diameter of 5 nm are embedded in the carbon nanofibers matrix(Fig. 3a and b). Fig. 3c displays the high resolution transmission electron microscopy (HRTEM) image and consequent fast Fourier transform (FFT) of Ni@C, in which the interplanar spacing of 0.207 nm is indexed to the (111) plane of Ni. In addition, the analogous selected area electron diffraction (SAED) pattern (Fig. 3d) confirms the crystalline structure of Ni, which is in good agreement with the XRD results and the HRTEM observation described above. The STEM and the corresponding energy-dispersive X-ray spectroscopy (EDS) elemental mappings further reveal the uniform dispersion of Ni particles within the carbon nanofibers in the Ni@C (Fig. 3e–g).
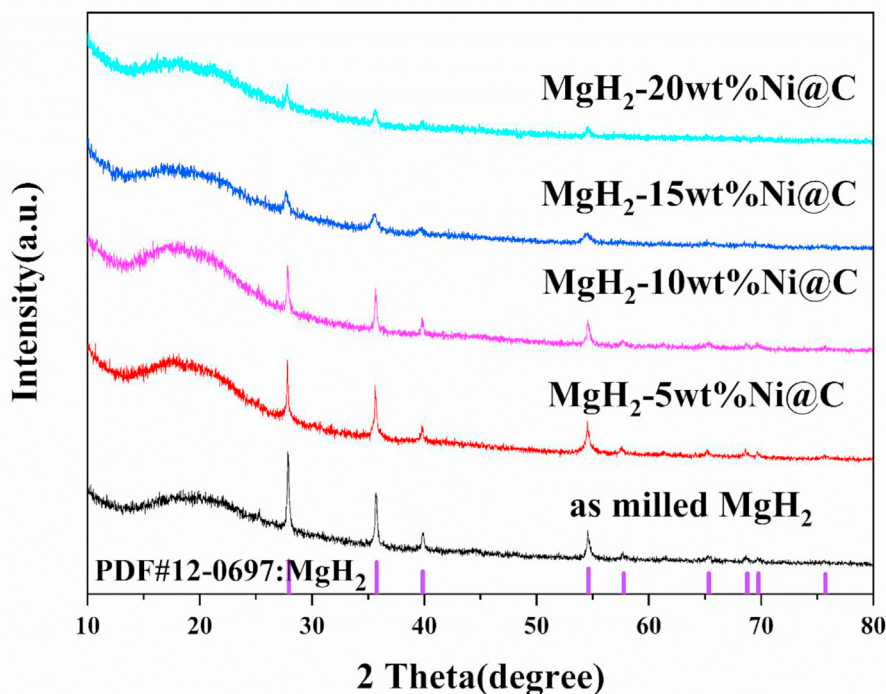
Fig. 4. XRD patterns of the as-milled MgH2 and MgH2-X wt%Ni@C (X = 5, 10, 15 and 20) composites.
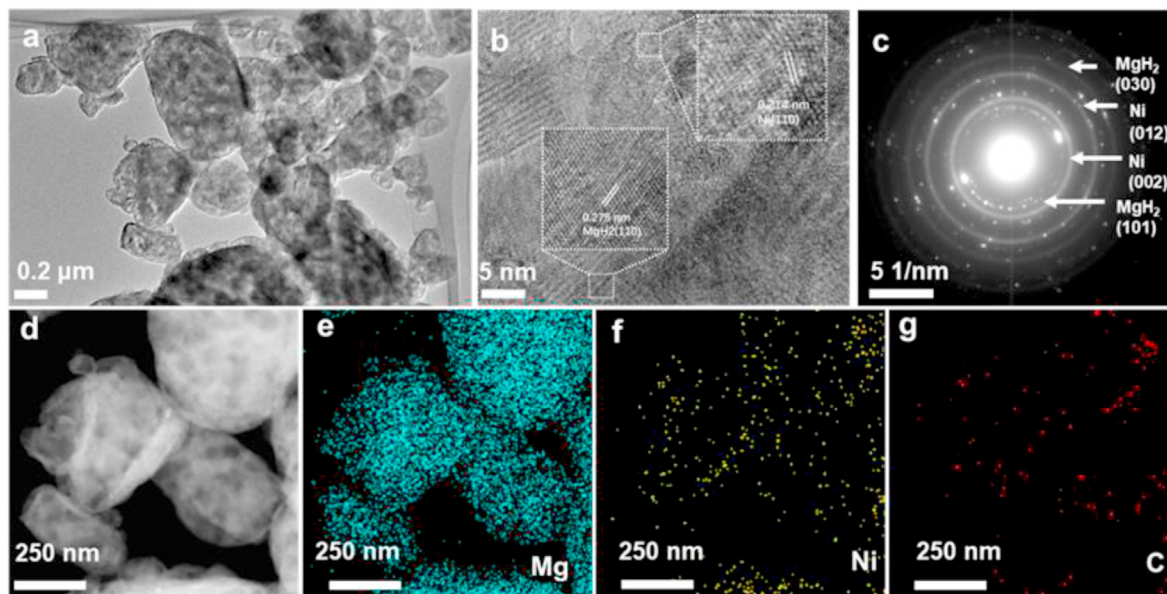

Fig. 5. (a) TEM image, (b) HRTEM image, (c) SAED pattern and (d−g) element mapping: (e) Mg, (f) Ni and (g) C of the MgH2-10 wt% Ni@C after ball milling.

The phase structures of as-milled MgH2, and MgH2-X wt%Ni@C (X = 5, 10, 15 and 20) samples are shown in Fig. 4. The XRD patterns of all the samples display the reflections of MgH2 phase. However, no reflection of Ni can be observed in all Ni-catalyzed samples because of small grain size of the synthesized Ni@C. Compared with the as-milled MgH2, the intensity of diffraction peak of MgH2 in all Ni-catalyzed nanocomposites decreases with the increased amount of Ni@C, caused by the poor crystallinity of the additive.

TEM studies were characterized to further investigate the microstructure of the MgH2-10 wt%Ni@C composite. Fig. 5a displays the image of MgH$_2$-10 wt%Ni@C composite with an uneven particle size of 200−500 nm. Fig. 5b illustrates the HRTEM image of the MgH2-10 wt%Ni@C composite, in which the lattice spacing of 0.275 nm corresponds to the (110) plane of MgH2 and the lattice spacing of 0.214 nm corresponds to the (110) plane of Ni. Furthermore, the diffraction rings (Fig. 5c) are identified to be the Ni and MgH2 phases, respectively, indicating the existence of Ni@C in the MgH2-10 wt%Ni@C composite. The EDX mappings of the MgH2-
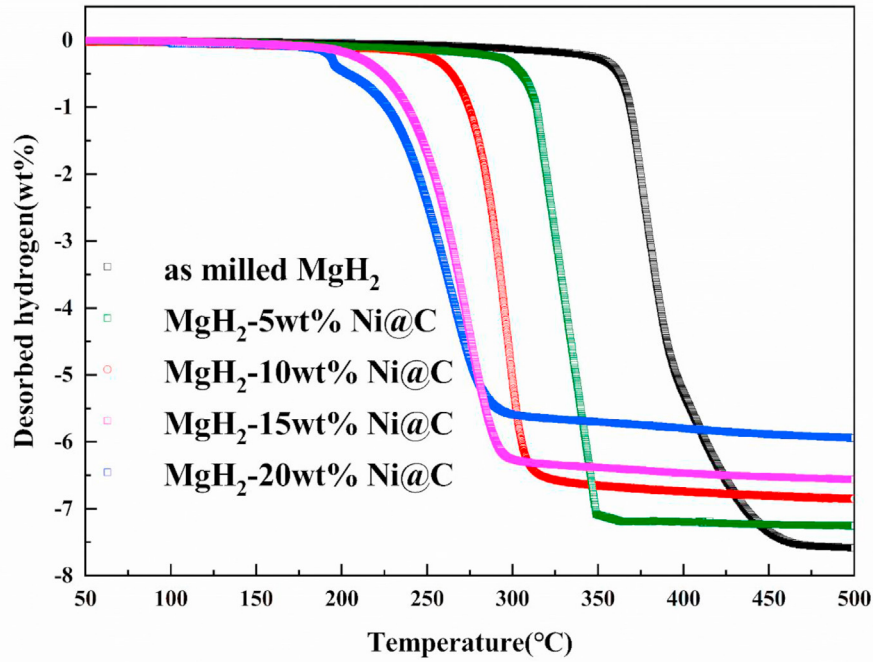
Fig. 6. TPD curves for ball-milled MgH2 and MgH2-X wt%Ni@C(X = 5, 10, 15 and 20) composites. The heating rate is 5 °C min-1.
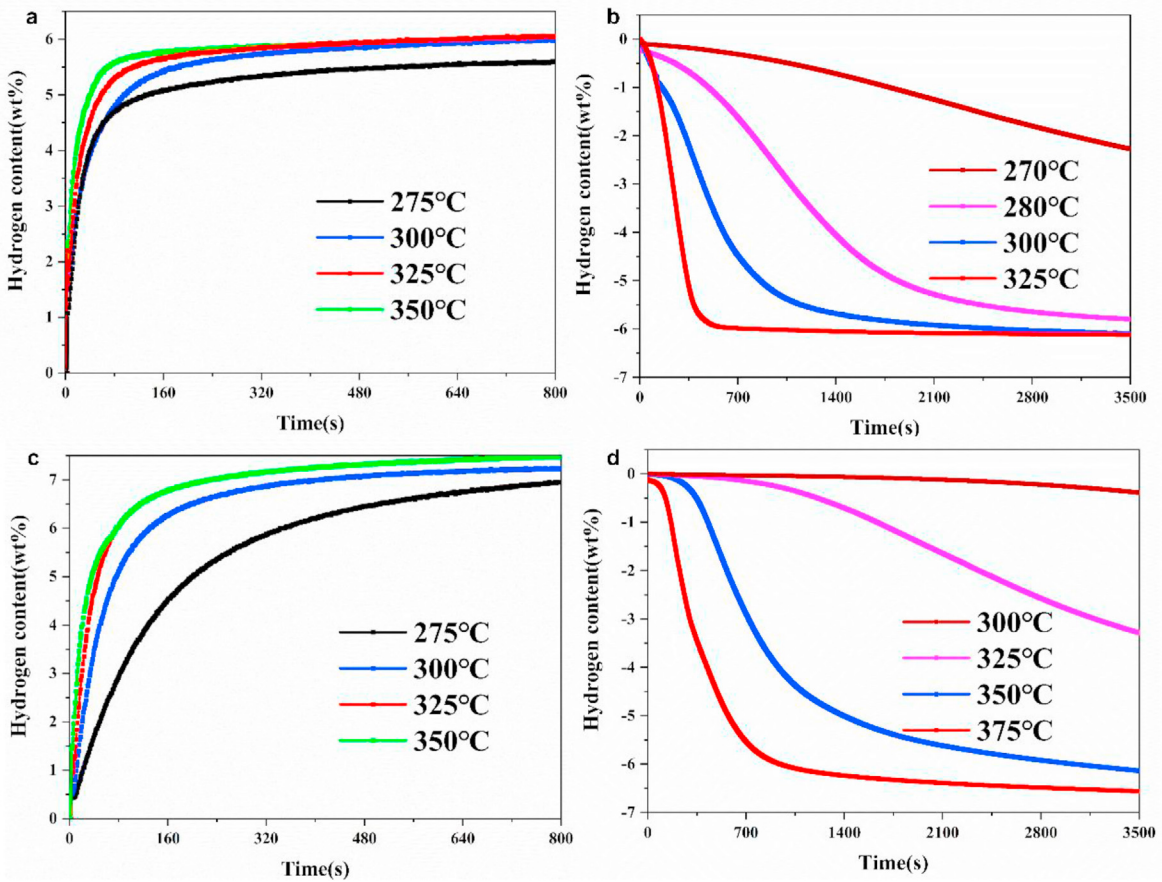

Fig. 7. Hydrogen absorption (a) and desorption (b) kinetics curves of MgH2-10 wt %Ni@C at different temperatures as compared with the hydrogen absorption (c) and desorption (d) kinetics curves of as-milled MgH2 at different temperatures.

Table 1
A comparison of apparent activation energies for dehydrogenation of Mg-based hydrogen storage systems.

Sample	E_a (kJ mol^{-1})	
	Sample	Comparative sample (pure MgH_2)
MgH_2-5 mol%Li_2TiO_3 [59]	84	113
$Mg_{17}Ba_2$ [60]	173.92	160
nfTa_2O_5−MgH_2 [61]	74 ± 7	143
$CeH_{2.73}$-MgH_2-Ni [62]	63 ± 3	158 ± 2
MgH_2/$NiCl_2$ [63]	102.6	158.5
This work	93.08	187.41

10 wt%Ni@C composite in Fig. 5d−g shows that the distribution of Ni@C in the MgH2 matrix is homogeneous.

3.2. Hydrogen storage performance of the MgH2− Ni@C sample

The dehydrogenation of MgH2 ball milled with different content of Ni@C is shown in Fig. 6. The onset dehydrogenation of MgH2-10 wt%Ni@C starts at 230 °C, which is 100 °C lower than that of as-milled MgH2. In addition, a hydrogen desorption capacity of 6.8 wt % can be reached on heating the MgH2-10 wt%Ni@C composite to 350 °C. In contrast, the as-milled MgH2 sample needs to be heated to 475 °C for a complete dehydrogenation. The onset and peak temperatures of dehydrogenation further shift to low temperature with the increasing Ni@C content in the composite, indicating that a high content addition of Ni@C has a positive effect on the desorption kinetics of MgH2. However, it is noticeable that the increasing Ni@C content will lead to a decreased dehydrogenation capacity. As a result, the MgH2-10 wt%Ni@C sample exhibited optimized dehydrogenation properties by simultaneously considering the operating temperature and the available hydrogen capacity in the present study.

To further study the hydrogenation/dehydrogenation kinetics of the MgH2-10 wt%Ni@C composite, isothermal sorption experiments of this sample as compared with the as-milled MgH2 were
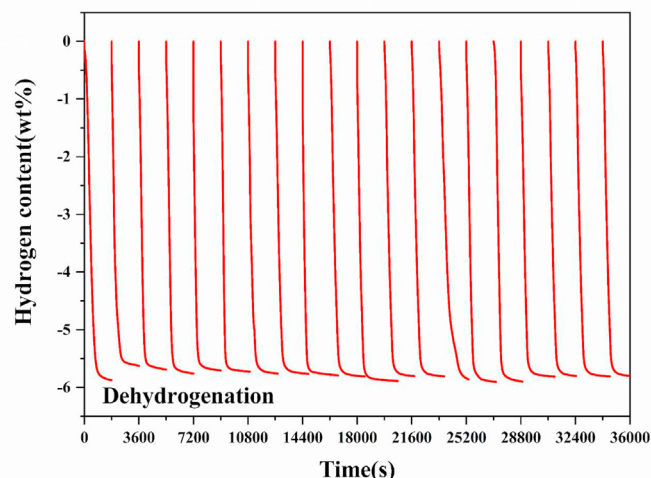

Fig. 9. Hydrogen desorption cycling curves of the MgH_2-10 wt%Ni@C composite at 325 °C.

measured at various temperatures, and the results are shown in Fig. 7. The hydrogen absorption kinetics curves show that the MgH2-10 wt %Ni@C composite has fast hydrogen absorption kinetics at temperatures ranging from 300 to 350 °C (Fig. 7a). The hydrogen absorption capacities can reach to 4.78 wt% and 5.60 wt% within 80 s at 300 °C and 350 °C, respectively. In contrast, as shown in Fig. 7c, the hydrogen absorption kinetics of as-milled MgH2 is sluggish before 300 °C, and to reach maximum hydrogen absorption capacity over 350 s at 350 °C is required. The desorption kinetics curves show that the MgH2-10 wt %Ni@C delivers hydrogen release of 5.79 wt% and 6.12 wt% at temperatures of 280 °C and 300 °C, respectively, whereas the as-milled MgH2 hardly decomposes at the same temperature (Fig. 7b, d). With the increase of operating temperature, MgH2-10 wt%Ni@C composite features
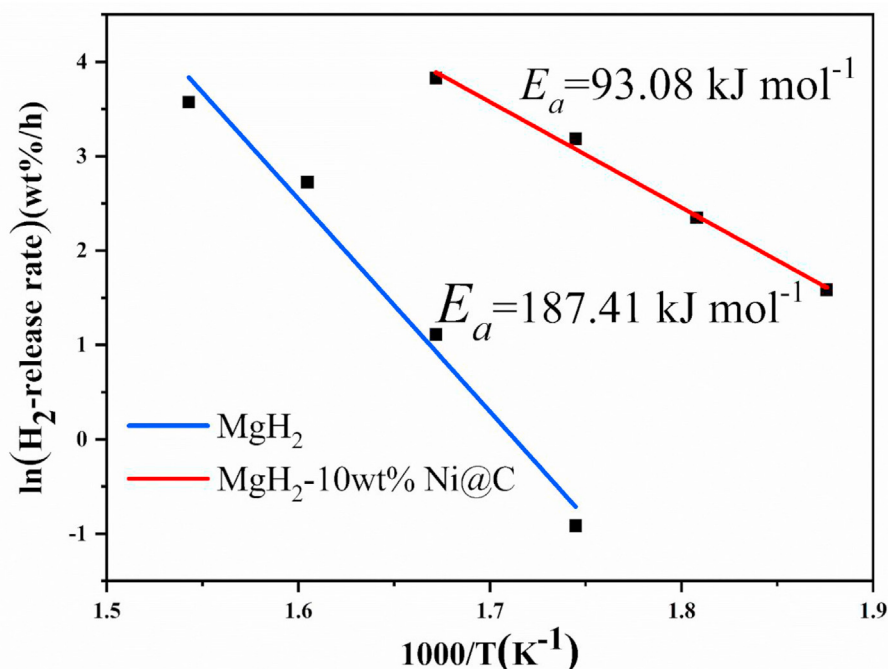

Fig. 8. Arrhenius plots according to the isothermal H2 desorption of MgH2-10 wt % Ni@C and the as-milled MgH2.
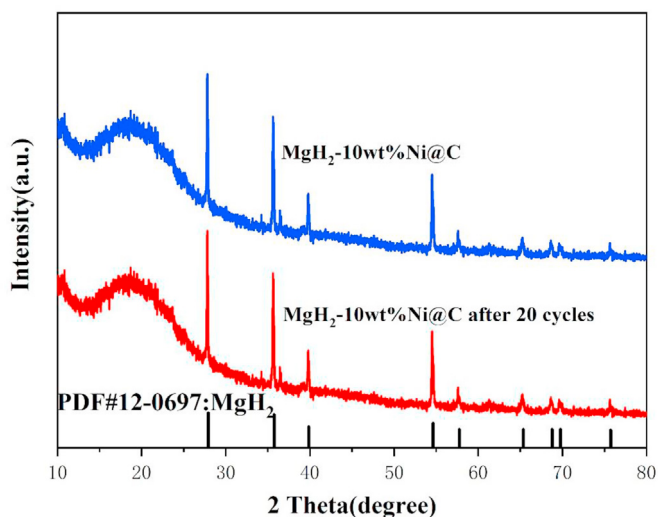
Fig. 10. XRD patterns of the MgH$_2$-10 wt%Ni@C before (a) and after (b) 20 hydrogen absorption/desorption cycles.

faster kinetics. At 325 °C, a hydrogen capacity of 5.91 wt% could be reached in 500 s. In contrast, the as-milled MgH2 can only release 0.03 wt% H2 at the same conditions. Even at a higher temperature of 375 °C the as-milled MgH2 can only release 4.55 wt% H2 at the same time. From the current experimental results, it can be concluded that Ni@C shows much better catalytic effect on improving the dehydrogenation of MgH2. The improved dehydriding kinetics can be further understood by calculating the apparent activation energy (Ea) during dehydrogenation at various temperatures. To show the catalytic effect of Ni@C on the dehydrogenation of MgH2 in terms of the activation energy, Table 1 gives a comparison of Ea of different Mg-based hydrogen storage systems. As shown in Fig. 8, by plotting ln(H2 release rate) versus T-1 [58], the Ea for desorption of MgH2-10 wt%Ni@C were determined to be 93.08 kJ mol−1, which are drastically lower than the

corresponding value for the as-milled MgH2 (187.41 kJ mol−1).

3.3. Cycling performance of the MgH$_2$-10 wt%Ni@C sample

Fig. 9 displays the hydrogen desorption cycling stability of MgH$_2$-10 wt%Ni@C composite at 325 °C. The dehydrogenation kinetics show no decrease during cycling. Meanwhile, around 99.8% of the initial capacity(5.86 wt% H$_2$)is preserved even after 20 cycles, exhibiting an excellent cyclic stability of the MgH$_2$-10 wt%Ni@C composite. Fig. 10 exhibits the XRD patterns of the MgH$_2$-10 wt%Ni@C sample before and after 20 hydrogen absorption/desorption cycles. It can be seen that both samples are mainly formed with MgH$_2$ phases. Ni is hardly detected before and after cycling due to its nanocrystalline states. The similarity XRD patterns of both samples verifies the good reversibility of the MgH$_2$-10 wt%Ni@C sample upon cycling.

Generally, the degradation of hydrogen storage properties of MgH$_2$ during hydrogenation-dehydrogenation cycles is caused by agglomeration of powders [64], growth of crystallites [65−67], and redistribution of catalysts [68]. To observe the microstructure stability, the MgH$_2$-10 wt%Ni@C composite was rehydrogenated at 300 °C and then characterized by TEM, HRTEM, SAED and EDS mapping after 20 hydrogen absorption/desorption cycles, as presented in Fig. 11. It displays that the MgH$_2$-10 wt%Ni@C composite maintains an uneven particle size of 200−500 nm and the average particle size shows no significant increase after cycling (Fig. 11a). According to the HRTEM image in Fig. 11b, the interplanar spacings of 0.204 nm and 0.151 nm corresponds to the (111) plane of Ni and the (002) plane of MgH$_2$, respectively. Furthermore, the diffraction rings (Fig. 11c) in SAED pattern are identified as belonging to Ni and MgH$_2$, which further proves the good reversibility of MgH$_2$ and the stability of Ni as an outstanding catalyst. Fig. 11d−g shows the corresponding elemental mapping results, which clearly illustrate the well distribution of Mg, Ni and C elements in the MgH$_2$-10 wt % Ni@C composite after 20 cycles, indicating that the Ni nanoparticles are still evenly distributed in the MgH$_2$-10 wt%Ni@C composite, accounting for the excellent hydrogenation and dehydrogenation kinetics and stable cycling of the MgH$_2$-10 wt%Ni@C composite. The
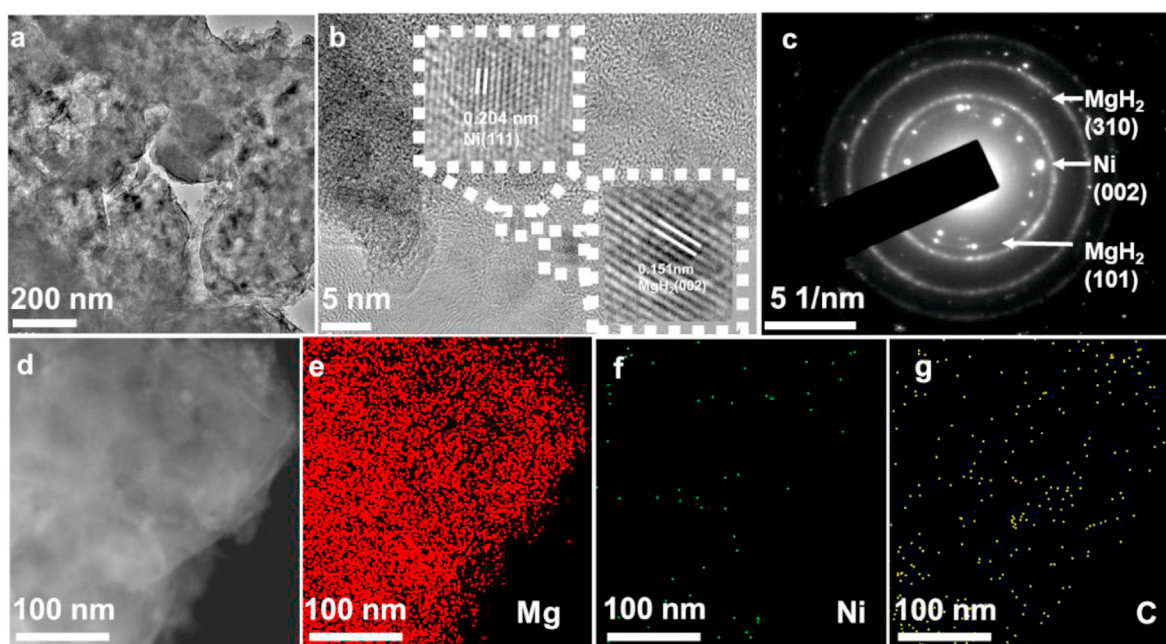

Fig. 11. (a) TEM image, (b) HRTEM image, (c) SAED pattern and (d−g) element mapping:(e) Mg, (f) Ni and (g) C of the MgH$_2$-10 wt%Ni@C after 20th rehydrogenation.

supported substrate (carbon nanofibers) plays an important role in preventing from further aggregating of catalytic Ni particles from each other during cycling at elevated temperatures and pressures, and thus the initial microstructural characteristics of the composites retain, leading to a reasonably good cyclic performance.

4. Conclusions

In summary, an electrospinning-based reduction approach is presented to generate nickel nanoparticles, which are protected from irreversible fusion and aggregation in subsequent high-temperature pyrolysis, in carbon nanofibers (Ni@C) in situ. The ultrafine Ni particles with an average size of 5 nm are embedded homogeneously in carbon fibers. The effect of the Ni@C on the structural and hydrogen storage performances of MgH_2 has been investigated systematically. The Ni@C catalyzed MgH_2 exhibited significantly improved hydrogen storage properties. It was demonstrated that the uniformly distributed ultrafine Ni nanoparticles in the MgH_2-10 wt%Ni@C composite are responsible for the superior catalytic effect of Ni@C, leading to the excellent hydrogenation and dehydrogenation kinetics and cycling performance of MgH_2.

CRediT authorship contribution statement

Qiufang Meng: designed experiments and carried out the experiments with assistance from Yuqin Huang, wrote original draft. **Yuqin Huang:** revised original draft. **Jikai Ye:** presented the figure of schematic illustration. **Guanglin Xia:** carried out the Supervision of research. **Gaofeng Wang:** carried out the supervision of research. **Linxi Dong:** carried out the supervision of research. **Zunxian Yang:** carried out the supervision of research. **Xuebin Yu:** conceived the concept of this work, revised original draft, carried out the supervision of research.

Declaration of competing interest

The authors declare that they have no known competing financial interests or personal relationships that could have appeared to influence the work reported in this paper.

Acknowledgements

References

[1] E. Rivard, M. Trudeau, K. Zaghib, Hydrogen storage for mobility: a review, Materials 12 (2019), https://doi.org/10.3390/ma12121973.

[2] R. Moradi, K.M. Groth, Hydrogen storage and delivery: review of the state of the art technologies and risk and reliability analysis, Int. J. Hydrogen Energy 44 (2019) 12254−12269.

[3] J.O. Abe, A.P.I. Popoola, E. Ajenifuja, O.M. Popoola, Hydrogen energy, economy and storage: review and recommendation, Int. J. Hydrogen Energy 44 (2019) 15072−15086.

[4] X. Yu, Z. Tang, D. Sun, L. Ouyang, M. Zhu, Recent advances and remaining challenges of nanostructured materials for hydrogen storage applications, Prog. Mater. Sci. 88 (2017) 1−48.

[5] J.F. Mao, X.B. Yu, Z.P. Guo, H.K. Liu, Z. Wu, J. Ni, Enhanced hydrogen storage performances of NaBH4-MgH2 system, J. Alloys Compd. 479 (2009) 619−623.

[6] A. Ranjbar, M. Ismail, Z.P. Guo, X.B. Yu, H.K. Liu, Effects of CNTs on the hydrogen storage properties of MgH2 and MgH2-BCC composite, Int. J. Hydrogen Energy 35 (2010) 7821−7826.

[7] Y. Wang, X. Chen, H. Zhang, G. Xia, D. Sun, X. Yu, Heterostructures built in metal hydrides for advanced hydrogen storage reversibility, Adv. Mater. 32 (2020), https://doi.org/10.1002/adma.202002647.

[8] X.B. Yu, D.M. Grant, G.S. Walker, A new dehydrogenation mechanism for reversible multicomponent borohydride systems-the role of Li-Mg alloys, Chem. Commun. 10.1039/b607869a(2006)3906-3908.

[9] X.B. Yu, Y.H. Guo, D.L. Sun, Z.X. Yang, A. Ranjbar, Z.P. Guo, H.K. Liu, S.X. Dou, A combined hydrogen storage system of Mg(BH4)2-LiNH2 with favorable dehydrogenation, J. Phys. Chem. C 114 (2010) 4733−4737.

[10] Y. Liu, K. Zhong, K. Luo, M. Gao, H. Pan, Q. Wang, Size-dependent kinetic enhancement in hydrogen absorption and desorption of the Li-Mg-N-H system, J. Am. Chem. Soc. 131 (2009) 1862−1870.

[11] Y. Pang, Y. Liu, M. Gao, L. Ouyang, J. Liu, H. Wang, M. Zhu, H. Pan, A mechanical-force-driven physical vapour deposition approach to fabricating complex hydride nanostructures, Nat. Commun. 5 (2014) 1−9.

[12] Y. Liu, H. Pan, M. Gao, Q. Wang, Advanced hydrogen storage alloys for Ni/MH rechargeable batteries, J. Mater. Chem. 21 (2011) 4743−4755.

[13] H. Pan, Y. Liu, M. Gao, Y. Zhu, Y. Lei, Q. Wang, An investigation on the structural and electrochemical properties of La0.7Mg0.3 (Ni0.85Co0.15) x (x= 3.15−3.80) hydrogen storage electrode alloys, J. Alloys Compd. 351 (2003) 228−234.

[14] H. Pan, Y. Liu, M. Gao, Y. Lei, Q. Wang, A study of the structural and electrochemical properties of La0.7Mg0.3 (Ni0.85Co0.15) x (x= 2.5 5.0) hydrogen storage alloys, J. Electrochem. Soc. 150 (2003) A565−A570.

[15] H. Pan, J. Ma, C. Wang, C. Chen, Q. Wang, Effect of Co content on the kinetic properties of the MlNi4.3-xCoxAl0.7 hydride electrodes, Electrochim. Acta 44 (1999) 3977−3987.

[16] B. Liao, Y. Lei, L. Chen, G. Lu, H. Pan, Q. Wang, Effect of the La/Mg ratio on the structure and electrochemical properties of LaxMg3−xNi9 (x= 1.6−2.2) hydrogen storage electrode alloys for nickel−metal hydride batteries, J. Power Sources 129 (2004) 358−367.

[17] S.G. Chalk, J.F. Miller, Key challenges and recent progress in batteries, fuel cells, and hydrogen storage for clean energy systems, J. Power Sources 159 (2006) 73−80.

[18] L. Ouyang, F. Qin, M. Zhu, The hydrogen storage behavior of Mg3La and Mg3LaNi0.1, Scripta Mater. 55 (2006) 1075−1078.

[19] M. Zhu, H. Wang, L.Z. Ouyang, M. Zeng, Composite structure and hydrogen storage properties in Mg-base alloys, Int. J. Hydrogen Energy 31 (2006) 251−257.

[20] L. Ouyang, X. Yang, H. Dong, M. Zhu, Structure and hydrogen storage properties of Mg3Pr and Mg3PrNi0.1 alloys, Scripta Mater. 61 (2009) 339−342.

[21] M. Ma, R. Duan, L. Ouyang, X. Zhu, Z. Chen, C. Peng, M. Zhu, Hydrogen storage and hydrogen generation properties of CaMg2-based alloys, J. Alloys Compd. 691 (2017) 929−935.

[22] L. Ouyang, Z. Cao, H. Wang, J. Liu, D. Sun, Q. Zhang, M. Zhu, Dual-tuning effect of in on the thermodynamic and kinetic properties of Mg2Ni dehydrogenation, Int. J. Hydrogen Energy 38 (2013) 8881−8887.

[23] Z. Cao, L. Ouyang, Y. Wu, H. Wang, J. Liu, F. Fang, D. Sun, Q. Zhang, M. Zhu, Dual-tuning effects of In, Al, and Ti on the thermodynamics and kinetics of Mg85In5Al5Ti5 alloy synthesized by plasma milling, J. Alloys Compd. 623 (2015) 354−358.

[24] L. Ouyang, Z. Cao, H. Wang, J. Liu, D. Sun, Q. Zhang, M. Zhu, Enhanced dehydriding thermodynamics and kinetics in Mg (In)−MgF2 composite directly synthesized by plasma milling, J. Alloys Compd. 586 (2014) 113−117.

[25] L.Z. Ouyang, Z.J. Cao, L.L. Li, H. Wang, J.W. Liu, D. Min, Y.W. Chen, F.M. Xiao, R.H. Tang, M. Zhu, Enhanced high-rate discharge properties of La11.3Mg6.0Sm7.4Ni61.0Co7.2Al7.1 with added graphene synthesized by plasma milling, Int. J. Hydrogen Energy 39 (2014) 12765−12772.

[26] M. Danaie, A.a.C. Asselli, J. Huot, G.A. Botton, Formation of the ternary complex hydride Mg2FeH6 from magnesium hydride (β-MgH2) and iron: an electron microscopy and energy-loss spectroscopy study, J. Phys. Chem. C 116 (2012) 25701−25714.

[27] J. Čermák, L. Král, Hydrogen diffusion in Mg-H and Mg-Ni-H alloys, Acta Mater. 56 (2008) 2677−2686.

[28] R. Janot, X. Darok, A. Rougier, L. Aymard, G.A. Nazri, J.M. Tarascon, Hydrogen sorption properties for surface treated MgH2 and Mg2Ni alloys, J. Alloys Compd. 404−406 (2005) 293−296.

[29] Y. Lei, Y. Wu, Q. Yang, J. Wu, Q. Wang, Electrochemical behaviour of some mechanically alloyed Mg-Ni-Based amorphous hydrogen storage alloys, Z. Phys. Chem. 183 (1994) 379−384.

[30] B. Liao, Y. Lei, L. Chen, G. Lu, H. Pan, Q. Wang, A study on the structure and electrochemical properties of La2Mg (Ni0.95M0.05)9 (M= Co, Mn, Fe, Al, Cu, Sn) hydrogen storage electrode alloys, J. Alloys Compd. 376 (2004) 186−195.

[31] Y. Jia, L. Cheng, N. Pan, J. Zou, G. Max Lu, X. Yao, Catalytic de/hydrogenation in Mg by Co-doped Ni and VOx on active carbon: extremely fast kinetics at low temperatures and high hydrogen capacity, Adv. Energy Mater. 1 (2011) 387−393.

[32] Y. Jia, C. Sun, Y. Peng, W. Fang, X. Yan, D. Yang, J. Zou, S.S. Mao, X. Yao, Metallic Ni nanocatalyst in situ formed from a metal−organic-framework by mechanochemical reaction for hydrogen storage in magnesium, J. Mater. Chem. A 3 (2015) 8294−8299.

[33] X. Huang, X. Xiao, W. Zhang, X. Fan, L. Zhang, C. Cheng, S. Li, H. Ge, Q. Wang, L. Chen, Transition metal (Co, Ni) nanoparticles wrapped with carbon and their superior catalytic activities for the reversible hydrogen storage of magnesium hydride, Phys. Chem. Chem. Phys. 19 (2017) 4019−4029.

[34] M.J. Liu, X.Z. Xiao, S.C. Zhao, S. Saremi-Yarahmadi, M. Chen, J.G. Zheng, S.Q. Li,

L.X. Chen, ZIF-67 derived Co@CNTs nanoparticles: remarkably improved hydrogen storage properties of MgH_2 and synergetic catalysis mechanism, Int. J. Hydrogen Energy 44 (2019) 1059−1069.

[35] Y.J. Kwak, S.H. Lee, B.S. Lee, H.R. Park, M.Y. Song, Enhancement of the hydrogen-storage properties of MgH_2 by the addition of Ni, $NaAlH_4$, Ti, and CNT via reactive mechanical grinding, J. Nanosci. Nanotechnol. 15 (2015), https://doi.org/10.1166/jnn.2015.11533.

[36] G. Xia, Y. Tan, X. Chen, D. Sun, Z. Guo, H. Liu, L. Ouyang, M. Zhu, X. Yu, Monodisperse magnesium hydride nanoparticles uniformly self-assembled on graphene, Adv. Mater. 27 (2015) 5981−5988.

[37] J.C. Crivello, B. Dam, R.V. Denys, M. Dornheim, D.M. Grant, J. Huot, T.R. Jensen, P. De Jongh, M. Latroche, C. Milanese, D. Milčius, G.S. Walker, C.J. Webb, C. Zlotea, V.A. Yartys, Review of magnesium hydride-based materials: development and optimisation, Appl. Phys. A 122 (2016), https://doi.org/10.1007/s00339-00016-09602-00330.

[38] Y.H. Sun, C.Q. Shen, Q.W. Lai, W. Liu, D.W. Wang, K.F. Aguey Zinsou, Tailoring magnesium based materials for hydrogen storage through synthesis: current state of the art, Energy Storage Mater 10 (2018) 168−198.

[39] C. Zlotea, C. Chevalier Cesar, E. Leonel, E. Leroy, F. Cuevas, P. Dibandjo, C. Vix Guterl, T. Martens, M. Latroche, Synthesis of small metallic Mg-based nanoparticles confined in porous carbon materials for hydrogen sorption, Faraday Discuss 151 (2011) 117−131.

[40] E.S. Cho, A.M. Ruminski, Y.S. Liu, P.T. Shea, S. Kang, E.W. Zaia, J.Y. Park, Y.D. Chuang, J.M. Yuk, X. Zhou, T.W. Heo, J. Guo, B.C. Wood, J.J. Urban, Hierarchically controlled inside-out doping of Mg nanocomposites for moderate temperature hydrogen storage, Adv. Funct. Mater. 27 (2017), 1704316.

[41] M. Chen, M. Hu, X. Xie, T. Liu, High loading nanoconfinement of V-decorated Mg with 1 nm carbon shells: hydrogen storage properties and catalytic mechanism, Nanoscale 11 (2019) 10045−10055.

[42] Y. Wang, Q.Y. Zhang, Y.J. Wang, L.F. Jiao, H.T. Yuan, Catalytic effects of different Ti-based materials on dehydrogenation performances of MgH_2, J. Alloys Compd. 645 (2015) S509−S512.

[43] H. Yu, S. Bennici, A. Auroux, Hydrogen storage and release: kinetic and thermodynamic studies of MgH_2 activated by transition metal nanoparticles, Int. J. Hydrogen Energy 39 (2014) 11633−11641.

[44] L. Xie, Y. Liu, X.Z. Zhang, J.L. Qu, Y.T. Wang, X.G. Li, Catalytic effect of Ni nanoparticles on the desorption kinetics of MgH_2 nanoparticles, J. Alloys Compd. 482 (2009) 388−392.

[45] M. Zhang, X. Xiao, J. Mao, Z. Lan, X. Huang, Y. Lu, B. Luo, M. Liu, M. Chen, L. Chen, Synergistic catalysis in monodispersed transition metal oxide nanoparticles anchored on amorphous carbon for excellent low-temperature dehydrogenation of magnesium hydride, Mater. Today Energy 12 (2019) 146−154.

[46] Z. Ma, J. Zhang, Y. Zhu, H. Lin, Y. Liu, Y. Zhang, D. Zhu, L. Li, Facile synthesis of carbon supported nano-Ni particles with superior catalytic effect on hydrogen storage kinetics of MgH_2, ACS Appl. Energy Mater. 1 (2018) 1158−1165.

[47] X. Huang, X. Xiao, W. Zhang, X. Fan, L. Zhang, C. Cheng, S. Li, H. Ge, Q. Wang, L. Chen, Transition metal (Co, Ni) nanoparticles wrapped with carbon and their superior catalytic activities for the reversible hydrogen storage of magnesium hydride, Phys. Chem. Chem. Phys. 19 (2017) 4019−4029.

[48] J. Chen, G. Xia, Z. Guo, Z. Huang, H. Liu, X. Yu, Porous Ni nanofibers with enhanced catalytic effect on the hydrogen storage performance of MgH_2, J. Mater. Chem. A 3 (2015) 15843−15848.

[49] X. Zhang, Y. Liu, X. Zhang, J. Hu, M. Gao, H. Pan, Empowering hydrogen storage performance of MgH_2 by nanoengineering and nanocatalysis, Mater. Today Nano 9 (2020), 100064.

[50] Y. Jia, C. Sun, Y. Peng, W. Fang, X. Yan, D. Yang, J. Zou, S.S. Mao, X. Yao, Metallic Ni nanocatalyst in situ formed from a metal-organic-framework by mechanochemical reaction for hydrogen storage in magnesium, J. Mater. Chem. A 3

[51] Z. Jalil, A. Rahwanto, Mursal Malahayati, E. Handoko, H. Akhyar, Hydrogen storage properties of mechanical milled MgH_2-nano Ni for solid hydrogen storage material, Mater. Sci. Eng. 432 (2018), 012034.

[52] L. Li, Z.C. Zhang, L.F. Jiao, H.T. Yuan, Y.J. Wang, In situ preparation of nanocrystalline Ni@C and its effect on hydrogen storage properties of MgH_2, Int. J. Hydrogen Energy 41 (2016) 18121−18129.

[53] L. Ouyang, Z. Cao, L. Li, H. Wang, J. Liu, D. Min, Y. Chen, F. Xiao, R. Tang, M. Zhu, Enhanced high-rate discharge properties of $La_{11.3}Mg_{6.0}Sm_{7.4}Ni_{61.0}Co_{7.2}Al_{7.1}$ with added graphene synthesized by plasma milling, Int. J. Hydrogen Energy 39 (2014) 12765−12772.

[54] C. Lin, L. Yang, L. Ouyang, J. Liu, H. Wang, M. Zhu, A new method for few-layer graphene preparation via plasma-assisted ball milling, J. Alloys Compd. 728 (2017) 578−584.

[55] C. Lin, L. Ouyang, C. Zhou, R. Hu, L. Yang, X. Yang, H. Shao, M. Zhu, A novel selenium-phosphorous amorphous composite by plasma assisted ball milling for high-performance rechargeable potassium-ion battery anode, J. Power Sources 443 (2019), 227276.

[56] M. Wang, C. Ye, H. Liu, M. Xu, S. Bao, Nanosized metal phosphides embedded in nitrogen-doped porous carbon nanofibers for enhanced hydrogen evolution at all pH values, Angew. Chem. 130 (2018) 1981−1985.

[57] S. Surendran, S. Shanmugapriya, A. Sivanantham, S. Shanmugam, R. Kalai Selvan, Electrospun carbon nanofibers encapsulated with NiCoP: a multifunctional electrode for supercapattery and oxygen reduction, oxygen evolution, and hydrogen evolution reactions, Adv. Energy Mater. 8 (2018), 1800555.

[58] X. Kang, Z. Fang, L. Kong, H. Cheng, X. Yao, G. Lu, P. Wang, Ammonia borane destabilized by lithium hydride: an advanced on-board hydrogen storage material, Adv. Mater. 20 (2008) 2756−2759.

[59] T. Zhang, S. Isobe, A. Jain, Y. Wang, S. Yamaguchi, H. Miyaoka, T. Ichikawa, Y. Kojima, N. Hashimoto, Enhancement of hydrogen desorption kinetics in magnesium hydride by doping with lithium metatitanate, J. Alloys Compd. 711 (2017) 400−405.

[60] D. Wu, L. Ouyang, C. Wu, Q. Gu, H. Wang, J. Liu, M. Zhu, Phase transition and hydrogen storage properties of $Mg_{17}Ba_2$ compound, J. Alloys Compd. 690 (2017) 519−522.

[61] S. Kumar, G.P. Tiwari, Thermodynamics and kinetics of MgH_2−$nfTa_2O_5$ composite for reversible hydrogen storage application, J. Mater. Sci. 52 (2017) 6962−6968.

[62] L. Ouyang, X. Yang, M. Zhu, J. Liu, H. Dong, D. Sun, J. Zou, X. Yao, Enhanced hydrogen storage kinetics and stability by synergistic effects of in situ formed $CeH_{2.73}$ and Ni in $CeH_{2.73}$-MgH_2-Ni nanocomposites, J. Mater. Chem. C 118 (2014) 7808−7820.

[63] J. Mao, Z. Guo, X. Yu, H. Liu, Z. Wu, J. Ni, Enhanced hydrogen sorption properties of Ni and Co-catalyzed MgH_2, Int. J. Hydrogen Energy 35 (2010) 4569−4575.

[64] B.S. Amirkhiz, B. Zahiri, P. Kalisvaart, D. Mitlin, Synergy of elemental Fe and Ti promoting low temperature hydrogen sorption cycling of magnesium, Int. J. Hydrogen Energy 36 (2011) 6711−6722.

[65] C.Q. Zhou, Y.Y. Peng, Q.G. Zhang, Growth kinetics of MgH_2 nanocrystallites prepared by ball milling, J. Mater. Sci. Technol. 50 (2020) 178−183.

[66] C. Zhou, Q. Zhang, Effect of Pr_3Al_{11} nanoparticles on crystallite growth kinetics of nanocrystalline Mg, J. Alloys Compd. 804 (2019) 299−304.

[67] C. Zhou, C. Hu, Y. Li, Q. Zhang, Crystallite growth characteristics of Mg during hydrogen desorption of MgH_2, Prog. Nat. Sci. 30 (2020) 246−250.

[68] S.D. House, J.J. Vajo, C. Ren, A.A. Rockett, I.M. Robertson, Effect of ball-milling duration and dehydrogenation on the morphology, microstructure and catalyst dispersion in Ni-catalyzed MgH_2 hydrogen storage materials, Acta Mater. 86 (2015) 55−68.